ACS Energy LETTERS

http://pubs.acs.org/journal/aelccp

# Enabling a Co-Free, High-Voltage $LiNi_{0.5}Mn_{1.5}O_4$ Cathode in All-Solid-State Batteries with a Halide Electrolyte

Jihyun Jang, Yu-Ting Chen, Grayson Deysher, Diyi Cheng, So-Yeon Ham, Ashley Cronk, Phillip Ridley, Hedi Yang, Baharak Sayahpour, Bing Han, Weikang Li, Weiliang Yao, Erik A. Wu, Jean-Marie Doux, Long Hoang Bao Nguyen, Jin An Sam Oh, Darren H. S. Tan, and Ying Shirley Meng*

Cite This: *ACS Energy Lett.* 2022, 7, 2531−2539

Read Online

ACCESS | Metrics & More | Article Recommendations | Supporting Information

**ABSTRACT:** One approach to increase the energy density of all-solid-state batteries (ASSBs) is to use high-voltage cathode materials. The spinel $LiNi_{0.5}Mn_{1.5}O_4$ (LNMO) cathode is one such example, as it offers a high reaction potential (close to 5 V). Moreover, it is a Co-free cathode system, which makes it an environmentally friendly and a low-cost alternative. However, several challenges must be addressed before it can be properly adopted in ASSB technologies. Herein, we reveal that lithium argyrodite ($Li_6PS_5Cl$), a sulfide solid-state electrolyte (SSE), possesses intrinsic chemical incompatibility with the LNMO cathode. We demonstrate the necessity of using a halide SSE, $Li_3YCl_6$ (LYC), through careful analysis of the LNMO/SSE interface. Moreover, we emphasize the necessity of applying a protective coating layer to LNMO particles, even when halide SSEs are used. Furthermore, the chemical phenomena involving LYC in the oxidative environment of LNMO are analyzed, including a comparison between coated and uncoated LNMO particles.

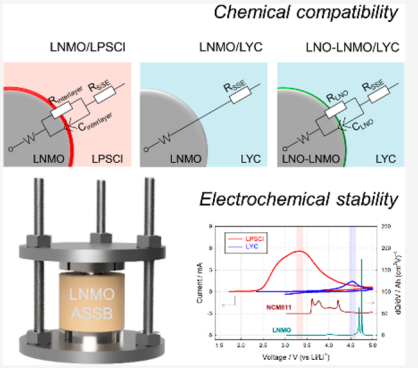


All-solid-state batteries (ASSBs) have been identified as a promising energy storage technology because of their prospects of nonflammability compared to organic liquid electrolytes.[1,2] To be integrated into portable electronics and electric transportation, aside from superior safety, ASSBs must meet the necessary performance metrics, which include both high energy and power density. Previously, layered oxides ($LiMO_2$, with M = Co, Ni, Mn, and/or Al) have been extensively investigated and have been shown to exhibit both high capacities and good capacity retention.[3−14] However, the high costs and supply chain uncertainties of raw Co materials have catalyzed the search for alternative cathode materials.[15−17] Thus, the cobalt-free $LiNi_{0.5}Mn_{1.5}O_4$ (LNMO) spinel cathode, which has a high operating voltage (~4.8 V vs $Li/Li^+$), is an attractive and cost-effective alternative for high energy density ASSBs. Previously, many studies have been conducted on the analysis of LNMO cathode material for current lithium-ion battery (LIB) systems and ways to improve their performance. The influence of transition metal ordering and the presence of $Mn^{3+}$ caused by oxygen vacancies affects the electrochemical behavior of the LNMO cell.[18−21] LNMO cycling in liquid LIBs inevitably induces continuous $Mn^{3+}$ production, which in turn produces soluble $Mn^{2+}$ through Jahn−Teller distortion and disproportionation reaction, causing cell degradation due to cross-talking.[22,23] Various approaches have been studied to improve cell performance by controlling the amount of $Mn^{3+}$, particle size, and crystallinity and by improving structural stability through doping.[24−28] Furthermore, many studies have been conducted on how to protect the LNMO surface through the application of various coating materials, such as metal oxide, organics, fluorides, and phosphates to prevent surface deterioration caused by an attack by HF generated from liquid electrolytes.[29−33] However, these degradation mechanisms inevitably occur because of the use of liquid electrolytes, which can be completely avoided in a solid-state electrolyte (SSE) system, thus representing an attractive approach for enabling the LNMO cathode material.

Among various SSE candidates in ASSB technologies, the argyrodite $Li_6PS_5Cl$ (LPSCl) is considered to be one of the leading materials in the industry because of its ease of manufacturing and high processability while retaining a relatively high ionic conductivity (>1 mS $cm^{-2}$ at 298

**Received:** June 18, 2022
**Accepted:** July 6, 2022







https://doi.org/10.1021/acsenergylett.2c01397
*ACS Energy Lett.* 2022, 7, 2531−2539

K).[3,34−36] However, sulfide-based SSEs still have drawbacks: (i) chemical instability with air/moisture which leads to SSE degradation and toxic $H_2S$ gas formation[37,38] and (ii) a narrow electrochemical stability window which can result in side reactions at both cathode and anode interfaces, resulting in increased cell resistance and irreversible capacity loss.[39−42] In particular, because the cathode must contain SSE particles in the electrode composite which inherently possesses more cathode material/SSE interfacial contact area, more significant effects due to side reactions occur.[3−5,7] Cathodes coated with oxides including lithium niobate ($LiNbO_3$, LNO), lithium borate, and lithium zirconate layers have been widely investigated to overcome this issue, and the type and quality of these coating layers have been shown to determine the overall performance of the cathode composite electrode.[8−12] In terms of high-voltage ASSBs, there have been a handful of previous efforts to introduce LNMO. Previously, Tatsumisago et al. and Hirayama et al. reported $Li_3PO_4$ (LPO) or LNO-coated LNMO and $Li_{10}GeP_2S_{12}$ (LGPS) for a cathode and SSE, which focused mainly on acetylene black/SSE and Li metal/SSE interfaces.[43−45] In addition, Yao et al. investigated the effect of the coating layer by utilizing $Li_4Ti_5O_{12}$, LPO, and LNO materials and by studying their effect on the performance of LNMO-ASSB cells.[46] Moreover, a sulfurized LNMO spinel cathode was also suggested, which suppressed interfacial side-reactions with sulfide SSE reported by Wu et al.[47] The specific evaluation conditions and results of these previous LNMO studies are shown in Table S1. However, they showed only very limited cycling performance (<20 cycles) with an incomplete investigation into the degradation mechanisms in the solid-state system. While the prevailing hypothesis reported in the literature revolves around the low oxidation stability limit of sulfide-based SSEs, the root causes still need to be thoroughly revealed by systematic analyses.

Contrary to sulfide-based SSEs, the halide-based SSEs have been recently popularized in cathode composites because of their higher oxidation stability limit compared to their sulfide counterparts.[4,48−51] Asano et al. were the first to report that low-crystalline $Li_3YCl_6$ (LYC) and $Li_3YBr_6$ halide SSEs had ionic conductivities of 0.51 and 0.72 mS $cm^{-1}$.[48] Various types of other halide SSEs that contain other transition metal ions such as In, Zr, and Sc have been discovered and found to exhibit suitable ionic conductivities with higher oxidative stability windows, thus enabling stable cycling performance of a >4 V class of cathode materials, including NCM cathodes without the protective coating layers.[52−59] However, experimental analysis of their decomposition and its products beyond the oxidation stability window as well as their application and performance limitations when used with higher-voltage (>4.8 V) cathode systems have yet to be explored. In this study, we first introduced LYC as the representative halide SSE in the LNMO cathode composite and compared the chemical compatibility between LNMO and LPSCl/LYC via electrochemical, spectroscopic, and electron microscopy methods. In addition, the degradation of halide at a high voltage around 4.5 V (vs $Li/Li^+$) was demonstrated, causing severe cell failure in the high-voltage regime. To overcome this, an amorphous LNO coating on LNMO is shown to be effective when combined with halide SSEs and is seen to be crucial for achieving improved cycling performance. It is experimentally demonstrated that the chemical compatibility and electrochemical stability should be considered for the choice of catholyte for ASSB-cathodes. In addition, we believe that the analytical approach in this study introduces the methodology of how to address the critical interfacial issues in high-voltage cathodes and provides new insights regarding their use in ASSB systems.

The chemical compatibility of LNMO with LPSCl was first investigated with symmetric cell electrochemical impedance spectroscopy (EIS) measurements of the cathode composite and compared to the same configuration where LPSCl was replaced with LYC (Figure 1). The physical properties including

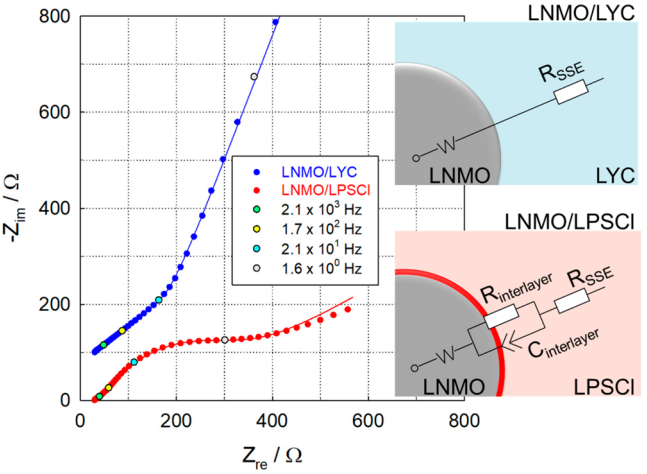


**Figure 1. Nyquist plots and corresponding equivalent circuits for LNMO/LPSCl and LNMO/LYC symmetric cells.**

the ionic and electronic conductivities of LPSCl and LYC used in the experiment are shown in Figure S1, which are $1.9 \times 10^{-3}$ and $2.8 \times 10^{-9}$ S $cm^{-1}$ and $0.4 \times 10^{-3}$ and $0.9 \times 10^{-9}$ S $cm^{-1}$ for LPSCl and LYC, respectively. Figure 1 shows the Nyquist plots of symmetric cells for a cathode composite consisting of LNMO, LPSCl, and vapor-grown carbon fiber (VGCF) (LNMO/LPSCl) and another of LNMO, LYC, and VGCF (LNMO/LYC). In the LNMO/LPSCl symmetric cell, a semicircle was observed around 21 Hz, whereas in the LNMO/LYC cell only the characteristic diffusion tail was observed. This difference in impedance behavior indicates the possibility that an interlayer between the LNMO and LPSCl, which corresponds to the semicircle, was generated during the composite mixing and pressing process. In addition, the difference between these two symmetric cells is more pronounced after 24 h (Figure S2), which emphasizes the chemical instability of LPSCl with LNMO. The detailed fitting results are included in Figure S2 and Table S2.

The physicochemical properties of both cathode composites were further studied in their pristine state before charging. Because analysis such as X-ray diffraction cannot detect the interface difference (Figure S3), X-ray photoelectron spectroscopy (XPS) and cross-sectional scanning electron microscopy (SEM) with focused-ion beam (FIB) were conducted to identify the possible interlayer species formed between LNMO and the SSE particles. As can be seen in Figure 2, the S 2p and P 2p XPS spectra of the LNMO/LPSCl composite (VGCF was not added) suggest that LPSCl decomposes into lithium sulfide ($Li_2S$), phosphorus pentasulfide ($P_2S_5$), polysulfides ($Li_2S_n$), and other phosphorus species.[4,7,40,60,61] It can be inferred that there is a chemical incompatibility between LNMO and LPSCl, which results in the generation of interlayers composed of decomposed LPSCl products. In stark contrast, only the $(YCl_6)^{3-}$ species is observed in the Y 3d XPS spectra of the


https://doi.org/10.1021/acsenergylett.2c01397
ACS Energy Lett. 2022, 7, 2531−2539

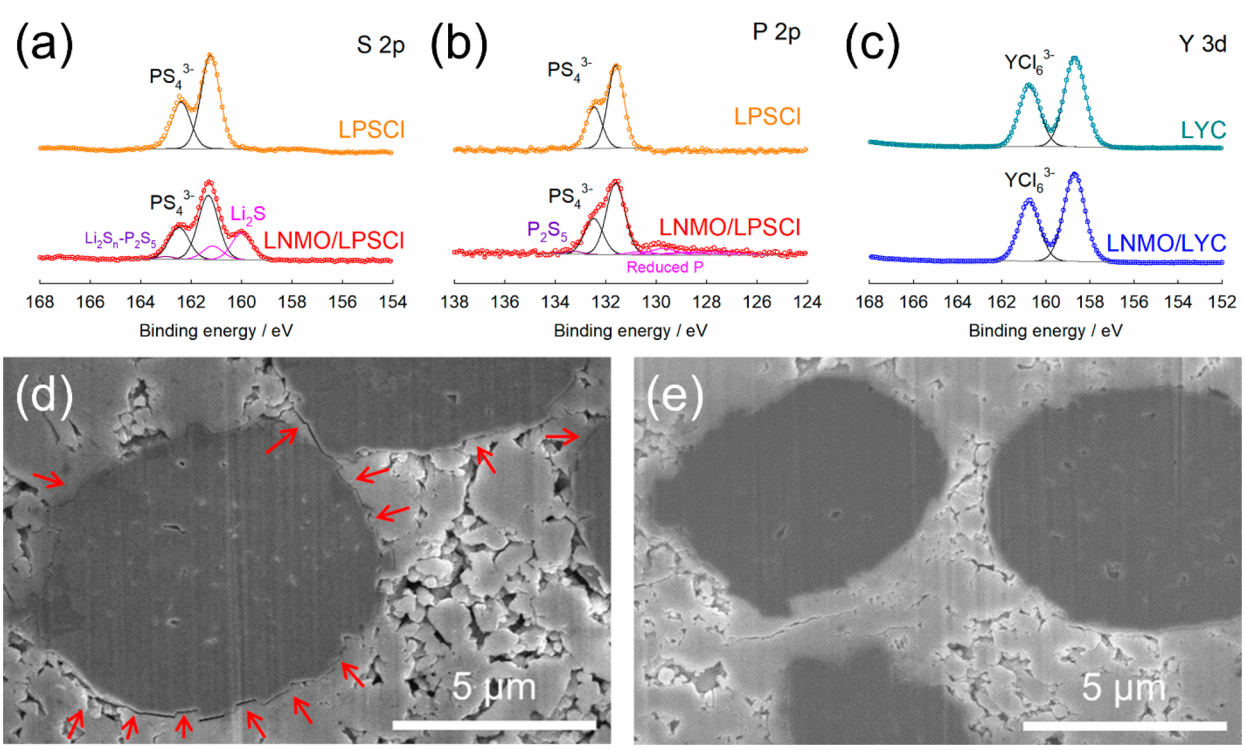


**Figure 2. (a) S 2p and (b) P 2p XPS spectra of LPSCl and LNMO/LPSCl composite. (c) Y 3d XPS spectra of LYC and LNMO/LYC composite. Cross-sectional SEM images of (d) LNMO/LPSCl and (e) LNMO/LYC composites. Note that those composites were obtained after only composite mixing and pressing (before charging).**

LNMO/LYC composite (Figure 2c), meaning no oxidation, nor reduction, of yttrium, which is in good agreement with the EIS results in Figure 1. In addition, a cross-sectional SEM image of the noncycled LNMO/LPSCl composite shows that there are interparticle voids at the interface, as indicated by arrows in Figure 2d. The formation of these voids was previously reported by Jung et al. after charging an oxide/LPSCl composite.[4] However, in this study the decomposition-driven contact loss in the LNMO/LPSCl composite is observed after only mixing and pressing. On the basis of the expected chemical decomposition reaction, the calculated molar volume of all decomposed products is smaller than that of LPSCl, which can explain the formation of interparticle voids in this composite (Table S3). On the other hand, good physical contact between LNMO and LYC is maintained in the LNMO/LYC composite (Figure 2e), which corresponds with no decomposed products in the Y 3d XPS (Figure 2c). The low-magnification cross-sectional images of both cathode composites are provided in Figure S4 for a clear comparison. With the physicochemical property comparisons, the incompatibility of LPSCl with LNMO even before cycling is demonstrated, and thus, it highlights the necessity of using halide-based SSE in the high-voltage LNMO cathode.

The electrochemical stability during the charge and discharge processes was examined. As shown in the cyclic voltammetry (CV) curve in Figure 3, LPSCl starts to oxidize at 2.5 V (vs Li/$Li^+$) during the positive scan, meaning it can be easily oxidized on the surface of most cathode materials. Comparing this CV curve with the d$Q$/d$V$ plot for the NCM811 shows that LPSCl would be oxidatively decomposed in the reaction voltage range of NCM811. On the other hand, LYC has a higher oxidation stability limit and a peak starts to occur around 4.3 V (vs Li/$Li^+$), beyond the upper voltage limit of the NCM811 cathode, which enables the use of NCM811 without coating. However, because

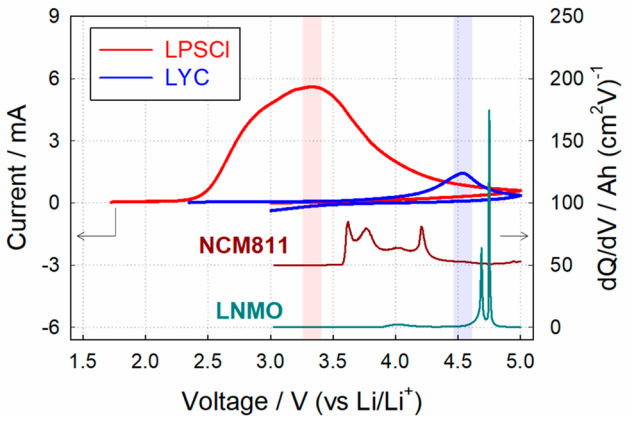


**Figure 3. CV curves for LPSCl/C and LYC/C composites all-solid-state half-cells, and the first cycle d$Q$/d$V$ plots for NCM811 and LNMO half-cells with liquid 1.0 M $LiPF_6$ in EC/EMC electrolyte.**

the reaction voltage of LNMO is higher than the oxidative stability limit of LYC, the LYC is expected to oxidatively decompose. Thus, an ionically conductive coating with even higher oxidation stability is still required to enable LNMO ASSBs.

To investigate the coating effect on the high-voltage LNMO cathode composite with LYC, the electrochemical performance of LNMO coated with 5 wt % LNO at 200 °C (LNO-LNMO) is compared with that of the pristine uncoated LNMO (Figure 4). The coating layer was confirmed as the amorphous LNO having a thickness of approximately 10−20 nm via XPS, XRD including high-temperature (500 °C) treated LNO-LNMO, high-angle annular dark-field (HAADF) image overlaid with the energy-dispersive X-ray spectroscopy (EDS) mapping, and EDS line


https://doi.org/10.1021/acsenergylett.2c01397
ACS Energy Lett. 2022, 7, 2531−2539

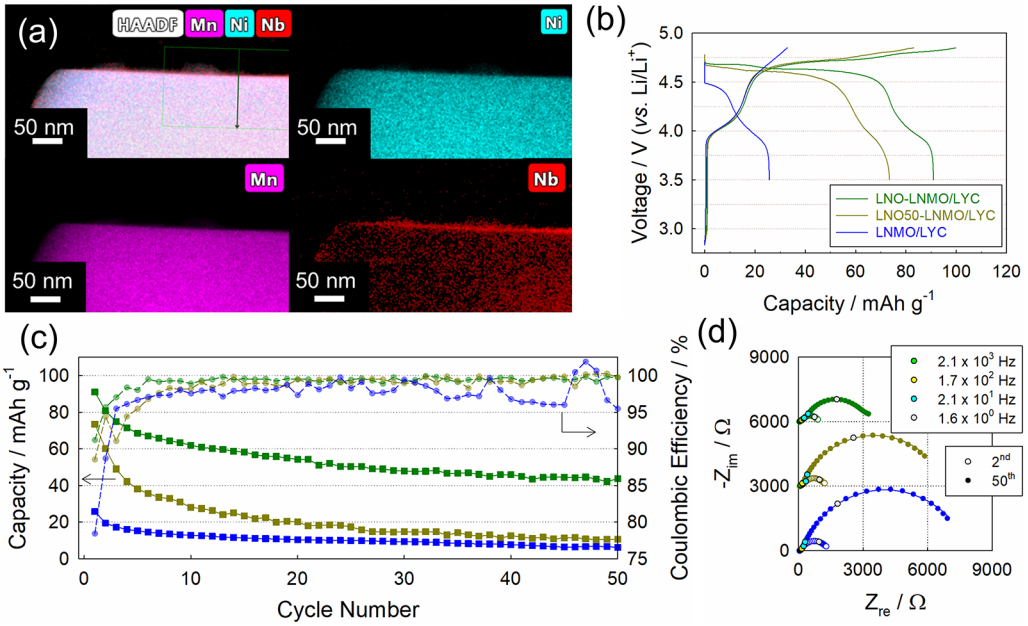


**Figure 4. (a) HAADF image of LNO-LNMO particle overlaid with EDS mapping and the corresponding elemental mappings of Ni, Mn, and Nb. (b) The first charge−discharge voltage profiles and (c) cycle performances and corresponding CEs of LNMO, LNO50-LNMO, and LNO-LNMO cathode cells at 7.5 and 20 mA $g^{-1}$, respectively. (d) Nyquist plots at the 2nd and 50th cycles of three cathode cells.**

scanning (Figures 4a and S5). Y 3d XPS spectra, symmetric cell EIS, and the cross-sectional SEM image for LNO-LNMO/LYC composite showed that LNO-LNMO is also stable in terms of chemical compatibility with LYC (Figure S6). Note that the semicircle at around 2.1 kHz in the symmetric cell EIS (Figure S6b) contains Li-ion conduction information within the LNO coating layer. Figure 4b shows the first cycle galvanostatic charge/discharge voltage profiles of LNMO/LYC and LNO-LNMO/LYC cells. In comparison with the LNMO/LPSCl cell (Figure S7), the parasitic reactions during the initial stage of charging are significantly reduced in LYC cells, which is mainly due to the higher stability of LYC in an oxidizing environment.[48,49] The LNMO/LYC cell exhibits only the $Mn^{3+}$ oxidation reaction from disordered LNMO structure at around 4 V (vs $Li/Li^+$)[16] without the $Ni^{2+}$ redox reaction above 4.5 V (vs $Li/Li^+$), resulting in the low first cycle charge/discharge capacities of 32.8/25.7 mAh $g^{-1}$ and an initial Coulombic efficiency (ICE) of 78.4% (Table S4). In stark contrast, the LNO-LNMO/LYC cell exhibits clear manganese and nickel redox reactions in the first cycle, showing charge/discharge capacities and an ICE of 99.7/91.0 mAh $g^{-1}$ and 91.2%, respectively (Table S4). Even though LYC has good chemical compatibility with LNMO and LNO-LNMO, the oxidation reaction at above 4.5 V (vs $Li/Li^+$) during the first cycle charging poses a different problem and will be discussed in detail later. Similar behavior is also observed in subsequent cycles (Figure 4c). The LNMO/LYC cell exhibited a capacity of <20 mAh $g^{-1}$ and considerably increased cell resistance after the 50th cycle, suggesting LNMO barely participated in the charge/discharge reaction because of higher cell polarization caused by LYC oxidation (Figures 4d and S8 and Table S5). This indicates that even LYC is not stable and oxidizes in the highly oxidative environment of LNMO (>4.5 V vs $Li/Li^+$). However, the LNO-LNMO/LYC cell shows reasonable cycle performance with stable CEs up to the 50th cycle, which is the highest performance for LNMO-ASSBs among the reported literature to date. The chemical compatibility and electrochemical performance of LNO-LNMO/LPSCl were also investigated (Figure S9). Symmetric cell EIS results show that LPSCl still can induce decomposition at the LNMO surface despite the presence of an LNO coating (Figure S9a) and was not able to perfectly protect the cathode during cycling, which results in the low initial capacity and poor cycle performance compared to the LNO-LNMO/LYC cell (Figure S9b,c). These electrochemical results imply that the intrinsic stability of the SSE itself and the use of a protective coating layer are both essential factors for enabling high-voltage cathode ASSBs. The symmetric cell EIS results and corresponding initial charge/discharge capacities according to the amount of LNO coating are indicated in Figure S10.

Because of the need for a protective coating layer, the effect of the coating characteristics on the electrochemical performance was also investigated and characterized. LNO-LNMO was compared with LNO-coated LNMO that had been annealed at 500 °C (LNO50-LNMO) (Figure 4). Figure 5 shows the high-resolution transmission electron microscopy (HR-TEM) images overlaid with inverse fast Fourier transform (FFT) and corresponding FFT patterns of the cross-section of LNO-LNMO and LNO50-LNMO prepared by the FIB. Note that there was a Pt deposition at the outside of the particle to protect the surface during FIB. In the coating layer of LNO-LNMO, the LNO lattice structure is not detected over the entire coating layer and only a distinct LNMO diffraction pattern is observed (Figure 5a). In contrast, there is a crystalline lattice structure of the LNO coating layer in LNO50-LNMO which corresponds to the LNO (012) plane (Figure 5b), in addition to the crystalline peak of $LiNbO_3$ in the XRD pattern of LNO50-LNMO (Figure S5e). The crystallinity of the coating layer can reduce both its ionic conductivity and coverage of the LNMO surface (Figure S11).[62] With increasing heating temperature, amorphous LNO starts to crystallize and aggregate, leading to lower ionic conductivity and less uniform coverage, which results in more direct contact between the cathode and LYC particles. Therefore, the LNO50-LNMO/LYC cell also cannot enable the full nickel redox reaction above 4.5 V (vs $Li/Li^+$), resulting in


https://doi.org/10.1021/acsenergylett.2c01397
ACS Energy Lett. 2022, 7, 2531−2539

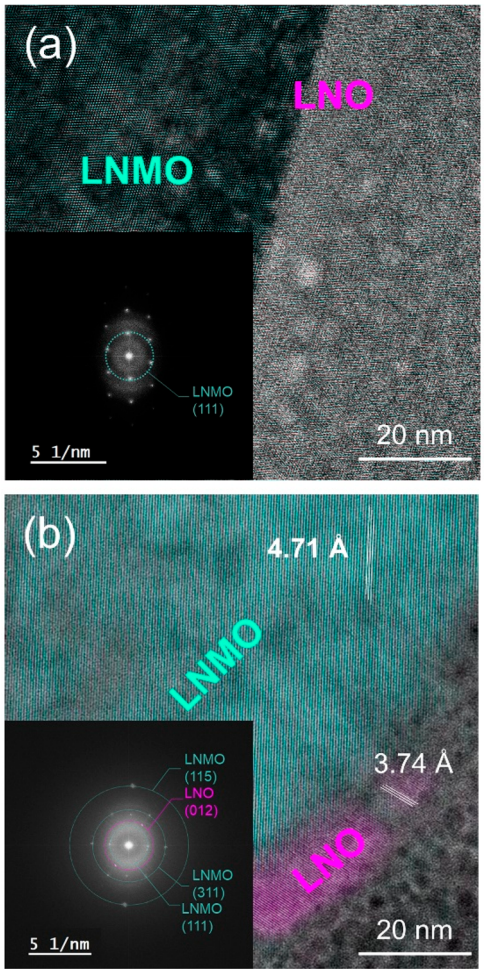


**Figure 5. HRTEM images overlaid with inverse FFT and corresponding FFT patterns of the cross section of (a) LNO-LNMO and (b) LNO50-LNMO.**

low initial capacity, cyclability, and high resistance after cycling (Figures 4 and S8 and Tables S4 and S5).

The role of the LNO coating layer was further determined by in situ EIS during the first cycle charge and discharge processes (Figure 6). As seen in the inset of Figure 6a, semicircles at a high frequency (170 Hz) and a low frequency (1.6 Hz) were observed in the LNMO/LYC cell at 4.0 V (vs $Li/Li^+$). To identify the origin of these two semicircles, the EIS results of the symmetric cell of the lithium−indium alloy (Li−In) anode were investigated (Figure S12a), and the Nyquist plot of this cell displays a semicircle at a low frequency, which means the low-frequency semicircle in a full-cell corresponds to the Li−In anode while the high-frequency semicircle is from cathode composite, especially the cathode electrolyte interphase, because the interfacial layer generally appears at a high frequency.[63−65] However, the resistance in the low-frequency region increases significantly above 4.5 V (vs $Li/Li^+$) and showed around 3000 Ω at 4.85 V (vs $Li/Li^+$). We also fabricated two symmetric cells containing charged cathode composites and charged Li−In anodes by disassembling identical full-cells after 4.85 V (vs $Li/Li^+$) charging (Figure S12a,b). The charged cathode symmetric cell showed a large semicircle at a low frequency which should be the charge-transfer resistance of the cathode,[63−65] while even reducing in the charged anode symmetric cell in comparison to the pristine state. The EIS results of both charged cathodes with fresh Li metal reference electrodes also were investigated to isolate the impedance measurements at each electrode separately, and the same trend was obtained (Figure S13). In summary, it can be interpreted that most of the resistance at a low frequency in a full-cell should stem from the increased charge-transfer resistance of the cathode composite driven by the oxidative decomposition of LYC. This is consistent with the electrochemical stability window (Figure 3) and the absence of the $Ni^{2+}$ oxidation reaction in the LNMO/LYC cell (Figure 4b). On the other hand, the LNO-LNMO/LYC cell initially shows a slightly larger resistance in the high-frequency region (~2.1 kHz) compared to the LNMO/LYC cell, which is largely due to the presence of the LNO coating layer. It shows significantly small resistance throughout the entire charge and discharge process while enabling the nickel redox reaction. This coating layer effectively reduces the oxidative decomposition reaction of LYC and prevents the formation of inactive species which hinder the lithium-ion conduction between LNMO and SSE, allowing the cell to be operated above 4.5 V (vs $Li/Li^+$). On the basis of the symmetric cell and full-cell analysis of cathode/anode before and after charging, the equivalent circuit containing two parallel RCs can be generated, and the fitted results of Figure 6 are shown in Figure S14 and Table S6.

The elemental analysis via HR-TEM revealed that the Cl/Y ratio of the SSE at the surface of LNMO changed from 6 to 3 after charging, which means LYC (Cl/Y ratio = 6) was decomposed to $YCl_3$ (Cl/Y ratio = 3) as expected by computational simulation,[49] while LYC was still maintained on the surface of LNO-LNMO (Figure S15 and Tables S7 and S8). In addition, the presence of pores between LNMO and LYC was also observed in the LNMO/LYC cathode composite after charging in the cross-sectional morphologies of the pelletized electrodes (Figure S16), which can be additional evidence of the oxidative decomposition reaction of LYC. These phenomena can contribute to the increased charge-transfer resistance of pristine LNMO and thus an improved initial capacity and cyclability of LNO-LNMO/LYC cathode composite in comparison with LNMO/LYC. As such, reducing the oxidative decomposition of the SSE during cycling and ensuring chemical and electrochemical compatibilities between LNMO and SSE are the main factors enabling the use of a high-voltage LNMO cathode in ASSBs.

In this study, the critical factors that must be addressed to enable high-voltage LNMO cathodes in ASSBs were investigated. It was confirmed that the LPSCl electrolyte, which is one of the most studied and promising sulfide SSEs, is chemically incompatible with LNMO, causing side reactions even during composite fabrication. On the other hand, LYC, a halide SSE with higher voltage stability, showed improved chemical compatibility with LNMO. However, it was observed that LYC still undergoes oxidative decomposition above 4.5 V (vs $Li/Li^+$) during charging, which results in the absence of the nickel redox reaction in LNMO. Therefore, a uniform and amorphous LNO layer coating on LNMO is needed for the improved utilization of nickel redox by mitigating the contribution of SSE oxidation which would increase cell resistance. This strategy showed improved lab-scale cell performance when compared to previous LNMO-ASSB studies, and this work establishes the methodology to investigate interfacial challenges regarding high-voltage cathodes and provides new insight toward enabling them for ASSBs.


https://doi.org/10.1021/acsenergylett.2c01397
ACS Energy Lett. 2022, 7, 2531−2539

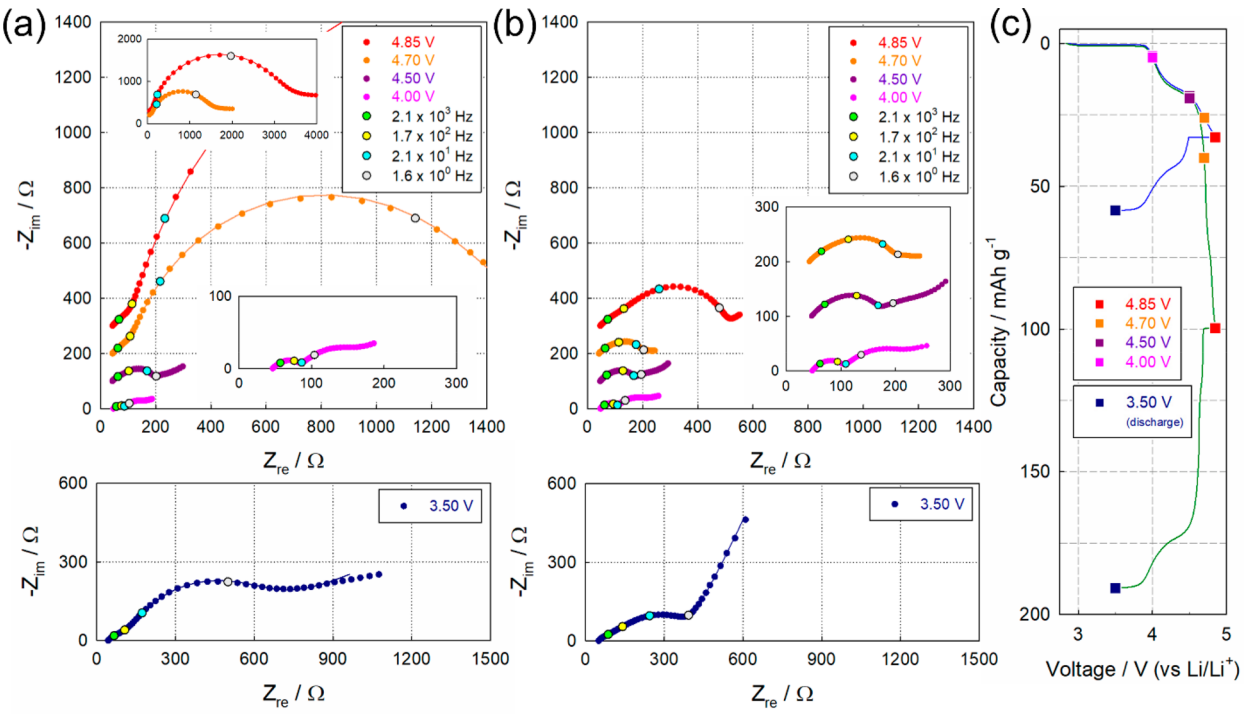


**Figure 6. Nyquist plots of (a) LNMO and (b) LNO-LNMO cathode cells at 4.0, 4.5, 4.7, and 4.85 V (vs $Li/Li^+$) during the first-cycle charge and 3.5 V (vs $Li/Li^+$) after the first-cycle discharge. (c) Cycling voltage profile of two cathode cells for reference.**

## ■ ASSOCIATED CONTENT

### Supporting Information

The Supporting Information is available free of charge at https://pubs.acs.org/doi/10.1021/acsenergylett.2c01397.

Experimental methods; ionic and electronic conductivities of LPSCl and LYC; Nyquist plots and corresponding fitted results; experimental data of cathodes and cathode composites, including XRD, powder SEM, FIB-SEM, XPS, HAADF, EIS, and additional electrochemical data (PDF)

## ■ AUTHOR INFORMATION


### Corresponding Author

**Ying Shirley Meng** − *Department of NanoEngineering, University of California San Diego, La Jolla, California 92093, United States; Pritzker School of Molecular Engineering, The University of Chicago, Chicago, Illinois 60637, United States*; Email: shirleymeng@uchicago.edu

### Authors

**Jihyun Jang** − *Department of NanoEngineering, University of California San Diego, La Jolla, California 92093, United States*; orcid.org/0000-0001-8438-140X

**Yu-Ting Chen** − *Materials Science and Engineering Program, University of California San Diego, La Jolla, California 92093, United States*; orcid.org/0000-0001-9525-8407

**Grayson Deysher** − *Materials Science and Engineering Program, University of California San Diego, La Jolla, California 92093, United States*; orcid.org/0000-0003-0482-8991

**Diyi Cheng** − *Materials Science and Engineering Program, University of California San Diego, La Jolla, California 92093, United States*; orcid.org/0000-0003-1616-9209

**So-Yeon Ham** − *Materials Science and Engineering Program, University of California San Diego, La Jolla, California 92093, United States*

**Ashley Cronk** − *Materials Science and Engineering Program, University of California San Diego, La Jolla, California 92093, United States*; orcid.org/0000-0001-6147-4662

**Phillip Ridley** − *Department of NanoEngineering, University of California San Diego, La Jolla, California 92093, United States*

**Hedi Yang** − *Department of NanoEngineering, University of California San Diego, La Jolla, California 92093, United States*

**Baharak Sayahpour** − *Materials Science and Engineering Program, University of California San Diego, La Jolla, California 92093, United States*

**Bing Han** − *Department of NanoEngineering, University of California San Diego, La Jolla, California 92093, United States*

**Weikang Li** − *Department of NanoEngineering, University of California San Diego, La Jolla, California 92093, United States*

**Weiliang Yao** − *Materials Science and Engineering Program, University of California San Diego, La Jolla, California 92093, United States*

**Erik A. Wu** − *Department of NanoEngineering, University of California San Diego, La Jolla, California 92093, United States*

**Jean-Marie Doux** − *Department of NanoEngineering, University of California San Diego, La Jolla, California 92093, United States*

**Long Hoang Bao Nguyen** − *Department of NanoEngineering, University of California San Diego, La Jolla, California 92093, United States*; orcid.org/0000-0001-7823-1595

**Jin An Sam Oh** − *Department of NanoEngineering, University of California San Diego, La Jolla, California 92093, United States;* orcid.org/0000-0001-9336-234X

**Darren H. S. Tan** − *Department of NanoEngineering, University of California San Diego, La Jolla, California 92093, United States*

Complete contact information is available at: https://pubs.acs.org/10.1021/acsenergylett.2c01397

### Notes

The authors declare no competing financial interest.

## ■ ACKNOWLEDGMENTS

This work was funded by the LG Energy Solution through Frontier Research Laboratory (FRL) program. The authors acknowledge the UCSD Crystallography Facility. This work was performed in part at the San Diego Nanotechnology Infrastructure (SDNI) of UCSD, a member of the National Nanotechnology Coordinated Infrastructure, which is supported by the National Science Foundation (Grant ECCS-1542148), along with the use of facilities and instrumentation supported by NSF through the UC San Diego Materials Research Science and Engineering Center (UCSD MRSEC), Grant #DMR-201192.

## ■ REFERENCES

(1) Jung, Y. S.; Oh, D. Y.; Nam, Y. J.; Park, K. H. Issues and Challenges for Bulk-Type All-Solid-State Rechargeable Lithium Batteries Using Sulfide Solid Electrolytes. *Isr. J. Chem.* **2015**, *55* (5), 472−485.

(2) Manthiram, A.; Yu, X.; Wang, S. Lithium Battery Chemistries Enabled by Solid-State Electrolytes. *Nature Reviews Materials* **2017**, *2* (4), 1610.

(3) Lee, Y. G.; Fujiki, S.; Jung, C.; Suzuki, N.; Yashiro, N.; Omoda, R.; Ko, D. S.; Shiratsuchi, T.; Sugimoto, T.; Ryu, S.; Ku, J. H.; Watanabe, T.; Park, Y.; Aihara, Y.; Im, D.; Han, I. T. High-Energy Long-Cycling All-Solid-State Lithium Metal Batteries Enabled by Silver−Carbon Composite Anodes. *Nature Energy* **2020**, *5* (4), 299−308.

(4) Han, Y.; Jung, S. H.; Kwak, H.; Jun, S.; Kwak, H. H.; Lee, J. H.; Hong, S. T.; Jung, Y. S. Single- or Poly-Crystalline Ni-Rich Layered Cathode, Sulfide or Halide Solid Electrolyte: Which Will Be the Winners for All-Solid-State Batteries? *Adv. Energy Mater.* **2021**, *11* (21), 2100126.

(5) Koerver, R.; Aygün, I.; Leichtweiß, T.; Dietrich, C.; Zhang, W.; Binder, J. O.; Hartmann, P.; Zeier, W. G.; Janek, J. Capacity Fade in Solid-State Batteries: Interphase Formation and Chemomechanical Processes in Nickel-Rich Layered Oxide Cathodes and Lithium Thiophosphate Solid Electrolytes. *Chem. Mater.* **2017**, *29* (13), 5574−5582.

(6) Tan, D. H. S.; Chen, Y. T.; Yang, H.; Bao, W.; Sreenarayanan, B.; Doux, J. M.; Li, W.; Lu, B.; Ham, S. Y.; Sayahpour, B.; Scharf, J.; Wu, E. A.; Deysher, G.; Han, H. E.; Hah, H. J.; Jeong, H.; Lee, J. B.; Chen, Z.; Meng, Y. S. Carbon-Free High-Loading Silicon Anodes Enabled by Sulfide Solid Electrolytes. *Science (1979)* **2021**, *373* (6562), 1494−1499.

(7) Banerjee, A.; Tang, H.; Wang, X.; Cheng, J. H.; Nguyen, H.; Zhang, M.; Tan, D. H. S.; Wynn, T. A.; Wu, E. A.; Doux, J. M.; Wu, T.; Ma, L.; Sterbinsky, G. E.; D'Souza, M. S.; Ong, S. P.; Meng, Y. S. Revealing Nanoscale Solid-Solid Interfacial Phenomena for Long-Life and High-Energy All-Solid-State Batteries. *ACS Appl. Mater. Interfaces* **2019**, *11* (46), 43138−43145.

(8) Sun, X.; Hori, S.; Li, Y.; Yamada, Y.; Suzuki, K.; Hirayama, M.; Kanno, R. Annealing-Induced Evolution at the LiCoO 2 /LiNbO 3 Interface and Its Functions in All-Solid-State Batteries with a Li 10 GeP 2 S 12 Electrolyte. *Journal of Materials Chemistry A* **2021**, *9* (7), 4117−4125.

(9) Jung, S. H.; Oh, K.; Nam, Y. J.; Oh, D. Y.; Brüner, P.; Kang, K.; Jung, Y. S. Li3BO3-Li2CO3: Rationally Designed Buffering Phase for Sulfide All-Solid-State Li-Ion Batteries. *Chem. Mater.* **2018**, *30* (22), 8190−8200.

(10) Wu, E. A.; Jo, C.; Tan, D. H. S.; Zhang, M.; Doux, J.-M.; Chen, Y.-T.; Deysher, G.; Meng, Y. S. A Facile, Dry-Processed Lithium Borate-Based Cathode Coating for Improved All-Solid-State Battery Performance. *J. Electrochem. Soc.* **2020**, *167* (13), 130516.

(11) Strauss, F.; Teo, J. H.; Maibach, J.; Kim, A. Y.; Mazilkin, A.; Janek, J.; Brezesinski, T. Li2ZrO3-Coated NCM622 for Application in Inorganic Solid-State Batteries: Role of Surface Carbonates in the Cycling Performance. *ACS Appl. Mater. Interfaces* **2020**, *12* (51), 57146−57154.

(12) Culver, S. P.; Koerver, R.; Zeier, W. G.; Janek, J. On the Functionality of Coatings for Cathode Active Materials in Thiophosphate-Based All-Solid-State Batteries. *Adv. Energy Mater.* **2019**, *9* (24), 1900626.

(13) Strauss, F.; Bartsch, T.; de Biasi, L.; Kim, A. Y.; Janek, J.; Hartmann, P.; Brezesinski, T. Impact of Cathode Material Particle Size on the Capacity of Bulk-Type All-Solid-State Batteries. *ACS Energy Letters* **2018**, *3* (4), 992−996.

(14) Jung, S. H.; Kim, U. H.; Kim, J. H.; Jun, S.; Yoon, C. S.; Jung, Y. S.; Sun, Y. K. Ni-Rich Layered Cathode Materials with Electrochemo-Mechanically Compliant Microstructures for All-Solid-State Li Batteries. *Adv. Energy Mater.* **2020**, *10* (6), 1903360.

(15) Li, M.; Lu, J. Cobalt in Lithium-Ion Batteries. *Science (1979)* **2020**, *367* (6481), 979−980.

(16) Li, W.; Cho, Y. G.; Yao, W.; Li, Y.; Cronk, A.; Shimizu, R.; Schroeder, M. A.; Fu, Y.; Zou, F.; Battaglia, V.; Manthiram, A.; Zhang, M.; Meng, Y. S. Enabling High Areal Capacity for Co-Free High Voltage Spinel Materials in next-Generation Li-Ion Batteries. *J. Power Sources* **2020**, *473*, 228579.

(17) Zhang, N.; Zaker, N.; Li, H.; Liu, A.; Inglis, J.; Jing, L.; Li, J.; Li, Y.; Botton, G. A.; Dahn, J. R. Cobalt-Free Nickel-Rich Positive Electrode Materials with a Core-Shell Structure. *Chem. Mater.* **2019**, *31* (24), 10150−10160.

(18) Yi, T. F.; Mei, J.; Zhu, Y. R. Key Strategies for Enhancing the Cycling Stability and Rate Capacity of LiNi0.5Mn1.5O4 as High-Voltage Cathode Materials for High Power Lithium-Ion Batteries. *J. Power Sources* **2016**, *316*, 85−105.

(19) Ryoo, H.; Bae, H. B.; Kim, Y.-M.; Kim, J.-G.; Lee, S.; Chung, S.-Y. Frenkel-Defect-Mediated Chemical Ordering Transition in a Li−Mn−Ni Spinel Oxide. *Angew. Chem., Int. Ed.* **2015**, *54* (27), 7963−7967.

(20) Song, J.; Shin, D. W.; Lu, Y.; Amos, C. D.; Manthiram, A.; Goodenough, J. B. Role of Oxygen Vacancies on the Performance of Li[Ni 0.5-XMn 1.5+ x]O 4 (x = 0, 0.05, and 0.08) Spinel Cathodes for Lithium-Ion Batteries. *Chem. Mater.* **2012**, *24* (15), 3101−3109.

(21) Chemelewski, K. R.; Lee, E. S.; Li, W.; Manthiram, A. Factors Influencing the Electrochemical Properties of High-Voltage Spinel Cathodes: Relative Impact of Morphology and Cation Ordering. *Chem. Mater.* **2013**, *25* (14), 2890−2897.

(22) Kim, J. W.; Kim, D. H.; Oh, D. Y.; Lee, H.; Kim, J. H.; Lee, J. H.; Jung, Y. S. Surface Chemistry of LiNi0.5Mn1.5O4 Particles Coated by Al2O3 Using Atomic Layer Deposition for Lithium-Ion Batteries. *J. Power Sources* **2015**, *274*, 1254−1262.

(23) Cho, J. H.; Park, J. H.; Lee, M. H.; Song, H. K.; Lee, S. Y. A Polymer Electrolyte-Skinned Active Material Strategy toward High-Voltage Lithium Ion Batteries: A Polyimide-Coated LiNi0.5Mn1.5O4 Spinel Cathode Material Case. *Energy Environ. Sci.* **2012**, *5* (5), 7124−7131.

(24) Luo, H.; Nie, P.; Shen, L.; Li, H.; Deng, H.; Zhu, Y.; Zhang, X. Synthesis of LiNi0.5Mn1.5O4 Hollow Microspheres and Their Lithium-Storage Properties. *ChemElectroChem.* **2015**, *2* (1), 127−133.

(25) Yin, C.; Zhou, H.; Yang, Z.; Li, J. Synthesis and Electrochemical Properties of LiNi0.5Mn1.5O4 for Li-Ion Batteries by the Metal-Organic Framework Method. *ACS Appl. Mater. Interfaces* **2018**, *10* (16), 13625−13634.

(26) Sha, O.; Wang, S.; Qiao, Z.; Yuan, W.; Tang, Z.; Xu, Q.; Su, Y. Synthesis of Spinel LiNi0.5Mn1.5O4 Cathode Material with Excellent

Cycle Stability Using Urea-Based Sol−Gel Method. *Mater. Lett.* **2012**, *89*, 251−253.
(27) Chen, M.; Hu, Z.; Wu, Z.; Hua, W.; Ozawa, K.; Gu, Q.; Kang, Y. M.; Guo, X.; Chou, S. L.; Dou, S. X. Understanding Performance Differences from Various Synthesis Methods: A Case Study of Spinel LiCr0.2Ni0.4Mn1.4O4 Cathode Material. *ACS Appl. Mater. Interfaces* **2016**, *8* (39), 26051−26057.
(28) Deng, Y. F.; Zhao, S. X.; Xu, Y. H.; Gao, K.; Nan, C. W. Impact of P-Doped in Spinel LiNi0.5Mn1.5O4 on Degree of Disorder, Grain Morphology, and Electrochemical Performance. *Chem. Mater.* **2015**, *27* (22), 7734−7742.
(29) Cho, H. M.; Chen, M. V.; MacRae, A. C.; Meng, Y. S. Effect of Surface Modification on Nano-Structured LiNi0.5Mn1.5O4 Spinel Materials. *ACS Appl. Mater. Interfaces* **2015**, *7* (30), 16231−16239.
(30) Xiao, B.; Liu, H.; Liu, J.; Sun, Q.; Wang, B.; Kaliyappan, K.; Zhao, Y.; Banis, M. N.; Liu, Y.; Li, R.; Sham, T.-K.; Botton, G. A.; Cai, M.; Sun, X. Nanoscale Manipulation of Spinel Lithium Nickel Manganese Oxide Surface by Multisite Ti Occupation as High-Performance Cathode. *Adv. Mater.* **2017**, *29* (47), 1703764.
(31) Zhao, R.; Li, L.; Li, Y. P.; Xu, T. H.; Pan, D.; Yu, C. Y.; Zhao, H. L.; Bai, Y. Decoration by Dual-Phase Li2ZrO3 Islands with Core−Shell Structures Enhances the Electrochemical Performance of High-Voltage LiNi0.5Mn1.5O4. *Appl. Phys. Lett.* **2020**, *116* (2), 021601.
(32) Fang, X.; Lin, F.; Nordlund, D.; Mecklenburg, M.; Ge, M.; Rong, J.; Zhang, A.; Shen, C.; Liu, Y.; Cao, Y.; Doeff, M. M.; Zhou, C. Atomic Insights into the Enhanced Surface Stability in High Voltage Cathode Materials by Ultrathin Coating. *Adv. Funct. Mater.* **2017**, *27* (7), 1602873.
(33) Xiao, B.; Liu, J.; Sun, Q.; Wang, B.; Banis, M. N.; Zhao, D.; Wang, Z.; Li, R.; Cui, X.; Sham, T.-K.; Sun, X. Unravelling the Role of Electrochemically Active FePO4 Coating by Atomic Layer Deposition for Increased High-Voltage Stability of LiNi0.5Mn1.5O4 Cathode Material. *Advanced Science* **2015**, *2* (5), 1500022.
(34) Yu, C.; van Eijck, L.; Ganapathy, S.; Wagemaker, M. Synthesis, Structure and Electrochemical Performance of the Argyrodite Li6PS5Cl Solid Electrolyte for Li-Ion Solid State Batteries. *Electrochim. Acta* **2016**, *215*, 93−99.
(35) Kim, D. H.; Lee, Y. H.; Song, Y. B.; Kwak, H.; Lee, S. Y.; Jung, Y. S. Thin and Flexible Solid Electrolyte Membranes with Ultrahigh Thermal Stability Derived from Solution-Processable Li Argyrodites for All-Solid-State Li-Ion Batteries. *ACS Energy Letters* **2020**, *5* (3), 718−727.
(36) Liu, G.; Shi, J.; Zhu, M.; Weng, W.; Shen, L.; Yang, J.; Yao, X. Ultra-Thin Free-Standing Sulfide Solid Electrolyte Film for Cell-Level High Energy Density All-Solid-State Lithium Batteries. *Energy Storage Materials* **2021**, *38*, 249−254.
(37) Park, K. H.; Bai, Q.; Kim, D. H.; Oh, D. Y.; Zhu, Y.; Mo, Y.; Jung, Y. S. Design Strategies, Practical Considerations, and New Solution Processes of Sulfide Solid Electrolytes for All-Solid-State Batteries. *Adv. Energy Mater.* **2018**, *8* (18), 1800035.
(38) Lee, D.; Park, K. H.; Kim, S. Y.; Jung, J. Y.; Lee, W.; Kim, K.; Jeong, G.; Yu, J. S.; Choi, J.; Park, M. S.; Cho, W. Critical Role of Zeolites as H2S Scavengers in Argyrodite Li6PS5Cl Solid Electrolytes for All-Solid-State Batteries. *Journal of Materials Chemistry A* **2021**, *9* (32), 17311−17316.
(39) Richards, W. D.; Miara, L. J.; Wang, Y.; Kim, J. C.; Ceder, G. Interface Stability in Solid-State Batteries. *Chem. Mater.* **2016**, *28* (1), 266−273.
(40) Tan, D. H. S.; Wu, E. A.; Nguyen, H.; Chen, Z.; Marple, M. A. T.; Doux, J. M.; Wang, X.; Yang, H.; Banerjee, A.; Meng, Y. S. Elucidating Reversible Electrochemical Redox of Li6PS5Cl Solid Electrolyte. *ACS Energy Letters* **2019**, *4*, 2418−2427.
(41) Banerjee, A.; Wang, X.; Fang, C.; Wu, E. A.; Meng, Y. S. Interfaces and Interphases in All-Solid-State Batteries with Inorganic Solid Electrolytes. *Chem. Rev.* **2020**, *120* (14), 6878−6933.
(42) Chen, Y.-T.; Marple, M. A. T.; Tan, D. H. S.; Ham, S.-Y.; Sayahpour, B.; Li, W.-K.; Yang, H.; Lee, J. B.; Hah, H. J.; Wu, E. A.; Doux, J.-M.; Jang, J.; Ridley, P.; Cronk, A.; Deysher, G.; Chen, Z.; Meng, Y. S. Investigating Dry Room Compatibility of Sulfide Solid-State Electrolytes for Scalable Manufacturing. *J. Mater. Chem. A* **2022**, *10*, 7155−7164.
(43) Yubuchi, S.; Ito, Y.; Matsuyama, T.; Hayashi, A.; Tatsumisago, M. 5 V Class LiNi0.5Mn1.5O4 Positive Electrode Coated with Li3PO4 Thin Film for All-Solid-State Batteries Using Sulfide Solid Electrolyte. *Solid State Ionics* **2016**, *285*, 79−82.
(44) Oh, G.; Hirayama, M.; Kwon, O.; Suzuki, K.; Kanno, R. Bulk-Type All Solid-State Batteries with 5 v Class LiNi0.5Mn1.5O4 Cathode and Li10GeP2S12 Solid Electrolyte. *Chem. Mater.* **2016**, *28* (8), 2634−2640.
(45) Oh, G.; Hirayama, M.; Kwon, O.; Suzuki, K.; Kanno, R. Effect of Surface Modification and Oxygen Deficiency on Intercalation Property of Lithium Nickel Manganese Oxide in an All-Solid-State Battery. *Solid State Ionics* **2016**, *288*, 244−247.
(46) Liu, G.; Lu, Y.; Wan, H.; Weng, W.; Cai, L.; Li, Z.; Que, X.; Liu, H.; Yao, X. Passivation of the Cathode-Electrolyte Interface for 5 V-Class All-Solid-State Batteries. *ACS Appl. Mater. Interfaces* **2020**, *12* (25), 28083−28090.
(47) Wang, Y.; Lv, Y.; Su, Y.; Chen, L.; Li, H.; Wu, F. 5V-Class Sulfurized Spinel Cathode Stable in Sulfide All-Solid-State Batteries. *Nano Energy* **2021**, *90*, 106589.
(48) Asano, T.; Sakai, A.; Ouchi, S.; Sakaida, M.; Miyazaki, A.; Hasegawa, S. Solid Halide Electrolytes with High Lithium-Ion Conductivity for Application in 4 V Class Bulk-Type All-Solid-State Batteries. *Adv. Mater.* **2018**, *30* (44), 1803075.
(49) Wang, S.; Bai, Q.; Nolan, A. M.; Liu, Y.; Gong, S.; Sun, Q.; Mo, Y. Lithium Chlorides and Bromides as Promising Solid-State Chemistries for Fast Ion Conductors with Good Electrochemical Stability. *Angew. Chem.* **2019**, *131* (24), 8123−8127.
(50) Li, X.; Liang, J.; Luo, J.; Norouzi Banis, M.; Wang, C.; Li, W.; Deng, S.; Yu, C.; Zhao, F.; Hu, Y.; Sham, T. K.; Zhang, L.; Zhao, S.; Lu, S.; Huang, H.; Li, R.; Adair, K. R.; Sun, X. Air-Stable Li 3 InCl 6 Electrolyte with High Voltage Compatibility for All-Solid-State Batteries. *Energy Environ. Sci.* **2019**, *12* (9), 2665−2671.
(51) Kwak, H.; Han, D.; Lyoo, J.; Park, J.; Jung, S. H.; Han, Y.; Kwon, G.; Kim, H.; Hong, S.; Nam, K.; Jung, Y. S. New Cost-Effective Halide Solid Electrolytes for All-Solid-State Batteries: Mechanochemically Prepared $Fe^{3+}$ -Substituted $Li_2ZrCl_6$. *Adv. Energy Mater.* **2021**, *11*, 2003190.
(52) Li, X.; Liang, J.; Luo, J.; Norouzi Banis, M.; Wang, C.; Li, W.; Deng, S.; Yu, C.; Zhao, F.; Hu, Y.; Sham, T. K.; Zhang, L.; Zhao, S.; Lu, S.; Huang, H.; Li, R.; Adair, K. R.; Sun, X. Air-Stable Li3InCl6 Electrolyte with High Voltage Compatibility for All-Solid-State Batteries. *Energy Environ. Sci.* **2019**, *12* (9), 2665−2671.
(53) Kwak, H.; Han, D.; Lyoo, J.; Park, J.; Jung, S. H.; Han, Y.; Kwon, G.; Kim, H.; Hong, S.-T.; Nam, K.-W.; Jung, Y. S. New Cost-Effective Halide Solid Electrolytes for All-Solid-State Batteries: Mechanochemically Prepared Fe3+-Substituted Li2ZrCl6. *Adv. Energy Mater.* **2021**, *11* (12), 2003190.
(54) Liang, J.; Li, X.; Wang, S.; Adair, K. R.; Li, W.; Zhao, Y.; Wang, C.; Hu, Y.; Zhang, L.; Zhao, S.; Lu, S.; Huang, H.; Li, R.; Mo, Y.; Sun, X. Site-Occupation-Tuned Superionic LixScCl3+ XHalide Solid Electrolytes for All-Solid-State Batteries. *J. Am. Chem. Soc.* **2020**, *142* (15), 7012−7022.
(55) Park, K. H.; Kaup, K.; Assoud, A.; Zhang, Q.; Wu, X.; Nazar, L. F. High-Voltage Superionic Halide Solid Electrolytes for All-Solid-State Li-Ion Batteries. *ACS Energy Letters* **2020**, *5*, 533−539.
(56) Zhou, L.; Zuo, T. T.; Kwok, C. Y.; Kim, S. Y.; Assoud, A.; Zhang, Q.; Janek, J.; Nazar, L. F. High Areal Capacity, Long Cycle Life 4 V Ceramic All-Solid-State Li-Ion Batteries Enabled by Chloride Solid Electrolytes. *Nature Energy* **2022**, *7* (1), 83−93.
(57) Kwak, H.; Wang, S.; Park, J.; Liu, Y.; Kim, K. T.; Choi, Y.; Mo, Y.; Jung, Y. S. Emerging Halide Superionic Conductors for All-Solid-State Batteries: Design, Synthesis, and Practical Applications. *ACS Energy Letters* **2022**, *7*, 1776−1805.
(58) Combs, S. R.; Todd, P. K.; Gorai, P.; Maughan, A. E. Editors' Choice—Review—Designing Defects and Diffusion through Substitutions in Metal Halide Solid Electrolytes. *J. Electrochem. Soc.* **2022**, *169* (4), 040551 DOI: 10.1149/1945-7111/AC5BAD.

(59) Liang, J.; Li, X.; Adair, K. R.; Sun, X. Metal Halide Superionic Conductors for All-Solid-State Batteries. *Acc. Chem. Res.* **2021**, *54* (4), 1023−1033.
(60) Auvergniot, J.; Cassel, A.; Ledeuil, J. B.; Viallet, V.; Seznec, V.; Dedryvère, R. Interface Stability of Argyrodite Li6PS5Cl toward LiCoO2, LiNi1/3Co1/3Mn1/3O2, and LiMn2O4 in Bulk All-Solid-State Batteries. *Chem. Mater.* **2017**, *29* (9), 3883−3890.
(61) Auvergniot, J.; Cassel, A.; Foix, D.; Viallet, V.; Seznec, V.; Dedryvère, R. Redox Activity of Argyrodite Li6PS5Cl Electrolyte in All-Solid-State Li-Ion Battery: An XPS Study. *Solid State Ionics* **2017**, *300*, 78−85.
(62) Sun, X.; Hori, S.; Li, Y.; Yamada, Y.; Suzuki, K.; Hirayama, M.; Kanno, R. Annealing-Induced Evolution at the $LiCoO_2$ /$LiNbO_3$ Interface and Its Functions in All-Solid-State Batteries with a $Li_{10}GeP_2S_{12}$ Electrolyte. *J. Mater. Chem. A* **2021**, *9*, 4117.
(63) Keefe, A. S.; Buteau, S.; Hill, I. G.; Dahn, J. R. Temperature Dependent EIS Studies Separating Charge Transfer Impedance from Contact Impedance in Lithium-Ion Symmetric Cells. *J. Electrochem. Soc.* **2019**, *166* (14), A3272−A3279.
(64) Yoon, T.; Soon, J.; Lee, T. J.; Ryu, J. H.; Oh, S. M. Dissolution of Cathode−Electrolyte Interphase Deposited on LiNi0.5Mn1.5O4 for Lithium-Ion Batteries. *J. Power Sources* **2021**, *503*, 230051.
(65) Choi, W.; Shin, H. C.; Kim, J. M.; Choi, J. Y.; Yoon, W. S. Modeling and Applications of Electrochemical Impedance Spectroscopy (EIS) for Lithium-Ion Batteries. *J. Electrochem. Sci. Technol.* **2020**, *11* (1), 1−13.


https://doi.org/10.1021/acsenergylett.2c01397
*ACS Energy Lett.* 2022, 7, 2531−2539